

CHAPTER 2

Pulse Amplification. The STRUT. Pulse Shaping.

2.1 Introduction

In this chapter, we begin by describing the technologies that are well established, and necessary to construct the amplified pulse shaping system. To study the shaped pulses that are described in later chapters, it is necessary to have a variety of pulse characterization tools. An autocorrelator, spectrometer and the STRUT (spectral and time resolved upconversion technique) were used for characterization. The STRUT is a technique that was recently developed, and this work shows for the first time its power and versatility. We also review other characterization techniques.

Next, we describe the amplified pulse system (without the pulse shaping) that was based on commercial technology. The system consists of a Ti:sapphire laser, a stretcher, regenerative amplifier, and compressor. We will discuss these components in detail. The center wavelength can be adjusted from 795 to 830nm, and the output pulse energy is 200 μ J at a repetition rate of 1kHz. The output beam had some spatial chirp which we removed by modifying the beam path. Except for some minor alterations, the system was not significantly altered from its original state. This means that researchers who would like to do amplified pulse shaping will be able to do so without modifying their existing amplification systems.

Throughout this project, we emphasized a modular system design. All components of this system were designed to be tested individually. For example, we used removable mirrors to allow us to study the system with various components removed from it.

We will then review previous work in pulse shaping. The AOM (acousto-optic modulator) pulse shaping technique has been previously demonstrated to shape over thirty features in the time domain. We will describe the experimental results from previous work.

2.2.1 Pulse Characterization

One of the underlying themes of this thesis will be the topic of pulse measurement. To those readers not familiar with ultrafast laser science, it may not be obvious why so much effort must be expended on measurement techniques. For cw (continuous wave) lasers, it is sufficient to use a spectrometer. Some pulsed lasers, such as the Nd:YAG laser, produce short pulses that have a duration of ns (nanoseconds). For such pulses, it is sufficient to use an oscilloscope or an auto-correlator.

For the ultrafast fs (femtosecond) pulses that we use, however, it is necessary to use more sophisticated techniques, described in detail below. These techniques include the FROG [1] (Frequency Resolved Optical Gating), the STRUT [2, 3] (Spectrally and Time Resolved Upconversion Technique), and the TADPOLE [4] (TADPOLE does not stand for anything!), and the SPIDER (neither does SPIDER) [5].

Most laser pulses are monochromatic. However, an ultrafast pulse has a wide optical bandwidth of over 8nm. It is this wide bandwidth that makes it an ultrafast pulse, which can be seen by taking the Fourier transform. It is also this wide optical bandwidth which makes it possible to do the pulse shaping work that will be described later. To describe such a pulse, we must find the function

$$E = A(\omega)\exp(i\mathbf{f}(\omega)) \quad (2.1)$$

The phase function $\mathbf{f}(\omega)$ gives us the phase of one frequency in the pulse with respect to another. For a monochromatic pulse, since there would only be one frequency, this phase function would not be necessary. Thus, to describe an ultrafast pulse, more information is required than to describe a monochromatic pulse. Just using a device such as a spectrometer will only give $A(\omega)$; to determine $\mathbf{f}(\omega)$ it is necessary to use a phase sensitive system.

An analogy that is very useful comes from music [6]. To describe a line of music, we use notes. The value of the note, (A through F) tells us what frequency to play it at, and the duration of the note tells us how long to hold it. The musical score will also tell us what order to play the notes in. This concept is shown in Fig.2-1, which is taken from [6].

2.2.2 Autocorrelator. Spectrometer.

Two types of autocorrelator were used in this project, each of which were useful for different pulse repetition rates. We used a speaker-design autocorrelator [7] to

study the Mira Ti:sapphire laser, which will be described later. The Mira has a pulse repetition rate of 77MHz, and since this repetition rate is much higher than the speaker frequency, the autocorrelator has no problem. An autocorrelator of the single-shot design [8], made by SpectraPhysics, was also used. This autocorrelator allowed us to study the 1kHz amplified pulses from the regenerative amplifier.

The spectrometer (made by Spex) was used with a grating groove density of 1200lines/mm or 1800lines/mm. The 1800lines/mm grating proved to be more suitable for our work because we needed the highest possible resolution to study the STRUT images. We calibrated it with a neon calibration lamp, and showed that it is accurate to within 0.5nm.

2.2.3 Advanced Pulse Characterization.

In this section, we describe advanced pulse characterization techniques. The spectrometer will give us the intensity as a function of frequency, $I(\omega)$. We will discuss cross-correlation, which has been used to study the shaped pulses in previous work, and gives the intensity as a function of time $I(t)$. Both of these techniques only give the intensity, and not the value of the field.

There are two main strategies for measuring the electric field [2]. One class of technique takes a two-dimensional representation of the one-dimensional electric field. The FROG and STRUT are members of this class. Another approach is to use spectral interferometry, which uses a one-dimensional scan. The spectral interferometric techniques include the TADPOLE and the SPIDER.

In previous work on shaped pulses [9], a cross-correlation technique was used to measure the pulse shape in the temporal domain. The cross-correlation is quite similar to the autocorrelation, except a reference pulse is used.

$$s(\mathbf{t}) \propto \int_{-\infty}^{\infty} dt I_{shaped}(t) \cdot I_{ref}(t - \mathbf{t}) \quad (2.1)$$

The cross-correlation is useful to measure shaped pulses for two reasons. First, the reference pulse is unshaped, so that the output signal is simpler than if an autocorrelation was performed. Second, the cross-correlation allows us to measure very weak pulses, because the reference pulse will be intense. Like the spectrometer, cross-correlation does not give phase information. Also, this measurement may be less sensitive than the spectrometer measurement. The reason is that the autocorrelation described above uses a 2nd harmonic generation crystal, so that it is a nonlinear process that requires a minimum intensity. So, this technique will not be effective at studying the signal-to-noise ratio of the pulse. The FROG and STRUT techniques described below also utilize the 2nd harmonic crystal, but the TADPOLE does not.

There are several variations on the FROG (frequency resolved optical grating), including the second harmonic generation (SHG) frog, and the polarization generation (PG) frog [1]. After we discuss the STRUT below, we will show that for a certain experimental setup of the STRUT, the STRUT and FROG are identical.

Like the FROG, the STRUT is a pulse characterization technique that allows us to characterize the pulse in amplitude and phase. The spectrometer only gives amplitude information, while the autocorrelator gives only temporal information. Although

the STRUT only uses intensity dependent detection devices (a diode array), it can still recover all the amplitude and phase information.

The setup is shown schematically in Fig.2-2. The STRUT has been discussed in previous work [2, 3], and here we will summarize the main equations. The input pulse is split up into two beams: the probe beam E_p and reference beam and E_r . The reference beam is spread spectrally and filtered by a rectangular slit, which has a filter function given by $G(\omega)$.

$$E_r = G(\mathbf{w})A(\mathbf{w})\exp(i\mathbf{f}(\mathbf{w})) \quad (2.2)$$

$$E_p = A(\mathbf{w})\exp(i\mathbf{f}(\mathbf{w})) \quad (2.3)$$

Let ω_{0r} be the central slit frequency, ω_1 be the distance away from that frequency, so that $\omega = \omega_{0r} + \omega_1$. The upconverted frequency is δ . The upconverted signal at the second harmonic crystal is given by:

$$E_{up}(\mathbf{d}) \propto \int_{-\infty}^{\infty} d\mathbf{w}_1 E_r(\mathbf{w}_{0r} + \mathbf{w}_1) \cdot E_p(\mathbf{d} - (\mathbf{w}_{0r} + \mathbf{w}_1)) \quad (2.4)$$

We may expand in a Taylor series about ω_{0r} assuming a narrow slit, where ω_{0r} is the center of the slit, and the frequency is $\omega = \omega_{0r} + \omega_1$.

$$E_p = A(\mathbf{d} - (\mathbf{w}_{0r} + \mathbf{w}_1))\exp[i\mathbf{f}(\mathbf{d} - (\mathbf{w}_{0r} + \mathbf{w}_1))] \quad (2.5)$$

$$E_r = G(\mathbf{w}_{0r})A(\mathbf{w}_{0r})\exp(i\mathbf{f}'(\mathbf{w}_{0r}) + \mathbf{w}_1) \quad (2.6)$$

$$E_p = A(\omega_0)\exp[i(\omega t - kx + \phi(\omega_0) + \omega \phi'(\omega_0))] \quad (2.7)$$

The probe beam is delayed by a time τ that is controlled by a delay stage.

$$E_p = A(\omega)\exp[i(\omega t - kx + \phi(\omega))] \exp[i\omega\tau] \quad (2.8)$$

The probe beam and reference beam are then combined in the second harmonic crystal.

The upconverted signal E_{up} is given by:

$$E_{up}(\mathbf{d}) \propto \int_{-\infty}^{\infty} d\mathbf{w}_1 E_r(\mathbf{w}_{or} + \mathbf{w}_1) \cdot E_p(\mathbf{d} - (\mathbf{w}_{or} + \mathbf{w}_1)) \cdot PM(\mathbf{w}_1) \quad (2.9)$$

With ω_1 considered to be small, we can make a Taylor approximation for the pulses.

$$\begin{aligned} E_p(\mathbf{d} - (\mathbf{w}_{or} + \mathbf{w}_1)) &= A(\mathbf{d} - \mathbf{w}_{or}) \exp[i\mathbf{f}(\mathbf{d} - \mathbf{w}_{or}) + i\mathbf{w}_1 \mathbf{f}'(\mathbf{d} - \mathbf{w}_{or})] \\ E_r(\mathbf{w}_{or} + \mathbf{w}_1) &= A(\mathbf{w}_{or}) \exp[i\mathbf{f}(\mathbf{w}_{or}) + i\mathbf{w}_1 \mathbf{f}'(\mathbf{w}_{or})] \end{aligned} \quad (2.10)$$

A delay stage is put on the probe stage that delays the pulse a time t , adding a phase factor to it.

$$E_p(\mathbf{d} - (\mathbf{w}_{or} + \mathbf{w}_1)) = A(\mathbf{d} - \mathbf{w}_{or}) \exp[i\mathbf{f}(\mathbf{d} - \mathbf{w}_{or}) + i\mathbf{w}_1 \mathbf{f}'(\mathbf{d} - \mathbf{w}_{or})] \exp[it(\mathbf{d} - (\mathbf{w}_{or} + \mathbf{w}_1))] \quad (2.11)$$

The upconverted signal becomes:

$$\begin{aligned} E_{up}(\mathbf{d}, t) &\propto A(\mathbf{d} - \mathbf{w}_{or}) A(\mathbf{w}_{or}) \exp[i\mathbf{f}(\mathbf{d} - \mathbf{w}_{or})] \exp[i\mathbf{f}(\mathbf{w}_{or})] \exp[it(\mathbf{d} - \mathbf{w}_{or})] \\ &\int_{-\infty}^{\infty} d\mathbf{w}_1 \exp[i\mathbf{w}_1 \mathbf{f}'(\mathbf{d} - \mathbf{w}_{or}) + i\mathbf{w}_1 \mathbf{f}'(\mathbf{w}_{or}) + it(\mathbf{d} - (\mathbf{w}_{or} + \mathbf{w}_1))] \end{aligned} \quad (2.12)$$

The spectrometer will see the intensity so the imaginary terms outside the integral drop out. We may also ignore terms that are not a function of δ or τ .

$$I(\mathbf{d}, t) \propto A^2(\mathbf{d} - \mathbf{w}_0) \left| \int d\mathbf{w}_1 \exp[i\mathbf{w}_1 \mathbf{f}'(\mathbf{d} - \mathbf{w}_{or}) + i\mathbf{w}_1 \mathbf{f}'(\mathbf{w}_{or}) + it\mathbf{w}_1] \right|^2 \quad (2.13)$$

This integral will be maximal when the condition is met that:

$$\mathbf{t} = \mathbf{f}'(\mathbf{d} - \mathbf{w}) + \mathbf{f}'(\mathbf{w}_{or}) \quad (2.14)$$

If we consider a certain frequency ω_p then:

$$f(\omega_p) = \int_{-\infty}^{\omega_p} d\omega [I(\omega + \omega_p)] \quad (2.15)$$

To find the amplitude we can integrate over time.

$$A^2(\omega_p) = \int dt [I(\omega_p + \omega_{0r}, t)] \quad (2.16)$$

This shows how the STRUT can recover both the amplitude and phase of the pulse. An important feature of the STRUT is that the algorithm is fast and does not require iteration.

It can also give the sign of the chirp.

In the beginning of this section, we mentioned the FROG. In the case where the slit of the STRUT is fully open, the STRUT is identical to the SHG (second harmonic generation) FROG. The equation describing this is Eq. (2.8), with $E_r = E_p$. In this case, the approximations that led to (2.14) and (2.16) are no longer valid. To recover the amplitude and phase, a complex iterative algorithm is necessary. We note that the STRUT, requires no iteration. In addition, for the SHG FROG, the sign of the chirp cannot be determined. That is, positive chirp (which corresponds to a sweep from lower frequency to higher frequency) cannot be distinguished from negative chirp. However, although the direction of the slope is indeterminate, the FROG will give the result that the pulse is chirped. Other versions of the FROG, are capable of giving the chirp direction. However, such FROG configurations require more complicated experimental setups [1].

Another intriguing measurement technique is the TADPOLE [4]. In this technique, a reference pulse is first characterized with the FROG. The STRUT could also be used to make this characterization. Then, the reference pulse and the shaped pulse are sent into a spectrometer, where they interfere. The resultant spectrum is known as the SI (spectral interference) spectrum.

$$I_{si}(\omega) = I_{ref}(\omega) + I_{unk}(\omega) + 2\sqrt{I_{ref}(\omega)I_{unk}(\omega)} \times \cos[\mathbf{f}_{unk}(\omega) - \mathbf{f}_{ref}(\omega) - \omega\tau]. \quad (2.17)$$

In this equation, I_{si} denotes the SI spectrum, I_{ref} denotes the reference pulse, and I_{unk} is the pulse to be determined, and τ is the time delay between the two pulses. Thus, we will do one measurement to determine $I_{unk}(\omega)$, and one measurement to determine the phase of the unknown pulse as in (2.15). By knowing the phase and amplitude of the reference pulse, we are able to determine the phase of the unknown pulse in one simple measurement. The necessary power for the TADPOLE is much lower than that for the STRUT, because no second harmonic crystal is necessary. Probably a technique such as the TADPOLE would have been useful in the unamplified pulse shaping done earlier. The TADPOLE may be a technique that we will pursue in further work.

There is one point that we should mention when considering the TADPOLE. As we will describe later, the Ti:sapphire laser produces a 76MHz pulsed beam. In contrast, the amplified pulse shaping system produces a 1kHz pulse beam. To do the TADPOLE measurement, it will be necessary to reduce the frequency of the Ti:sapphire laser to 1kHz, to match the amplified beam. A possible setup is shown schematically in Fig.2-3. The amplified pulse shaping system is shown as a black box with two outputs. The first output is the shaped pulse at a 1kHz repetition rate. The amplified pulse shaping system also has as output a weak beam which has the 76MHz repetition rate of the Ti:sapphire laser. There is an AOM in the path of the weak beam that reduces the repetition rate to 1kHz. The weak beam is then interfered with the amplified beam. This setup may be useful for pump-probe geometries that we will mention later.

Finally, we mention the SPIDER [5]. Like the TADPOLE, the SPIDER uses spectral interferometry. However, while the TADPOLE uses a reference pulse, the

SPIDER uses the same pulse that had been frequency shifted by a shift Ω . This frequency shift is typically 5-10% of the input spectral bandwidth, and can be generated by using an arrangement similar to the stretcher, along with a 2nd harmonic crystal.

In this section, we have discussed the STRUT, the FROG, the TADPOLE, and the SPIDER. In later chapters of this thesis, we will use the STRUT to analyze complex shaped pulses.

2.3.1 Pulse Amplification System

The amplification system is shown schematically in Fig.2-4, and is composed of commercially available components [10]. The first laser, an argon laser, pumps a Ti:sapphire laser. The Ti:sapphire laser is modelocked and then goes into a stretcher, which stretches the pulse in time. The regenerative amplifier then amplifies the beam and then the compressor compresses it to its original pulse length.

The first laser in the system is an Argon-ion laser, the Coherent INNOVA 200. This laser generates 8W of CW power at a wavelength of 514nm. We operate this laser in the multi-line mode, with an aperture setting of 8. The PowerTrack setting automatically adjusts the mirrors in the laser to maintain optimum power. Stability of the Argon laser is critical to the stability of the Ti:sapphire laser.

The Argon-ion laser pumps a Coherent Mira Ti:sapphire laser. The Mira is modelocked and produces an output beam that is tunable from 780-830nm, with average power of 1W. The 77MHz repetition rate of this laser is determined by the cavity length. The pulse length is about 120fs, and the spectral bandwidth is 10nm. An auto-correlator of

the speaker design was used to measure this pulsewidth. Fig.2-5a shows the Ti:sapphire signal that is taken from a photodiode inside the laser. On a scale of 50ns, we can see a set of spikes corresponding to each pulse of the laser. On a scale of 1ms we should see a straight line, as shown in Fig.2-5b. When the Ti:sapphire is not correctly adjusted we can see giant pulses, as shown in Fig.2-5c. These pulses will cause instability in the later parts of the system, such as the regenerative amplifier, and the Ti:sapphire must be adjusted to the mode in Fig.2-5b.

The amplification system, including the stretcher, regenerative amplifier, and compressor, works on the chirped pulse amplification principle [11], and is manufactured by CLARK-MXR [10]. The Ti:sapphire beam is sent into the stretcher, which acts to stretch the beam in time but not changing its spatial profile. This stretching is necessary to reduce the peak intensity of the input laser, for too high a peak intensity will damage the regenerative amplifier. The stretcher stretches the beam to 150ps.

Fig.2-6 shows a schematic of a 4-F system, which is the grating-lens setup used extensively in this project. This setup, with modifications, is at the heart of the pulse shaper, stretcher, and compressor. Fig.2-6 shows the transverse beam profile as it travels through a generalized 4-F system.

The regenerative amplifier is itself a Ti:sapphire laser that is pumped by a Nd:YAG laser. The Nd:YAG laser is Q-switched at a frequency of 1kHz, producing 512nm light pulses with a total power of 10W. It was not necessary to change the amplifier in this project, so we will not show complete diagrams. The Q-switching allows the Ti:sapphire crystal to produce a large amount of energy in a short time, even though it is not modelocked. The incoming pulse from the stretcher is referred to as the seed pulse.

It is necessary for the seed pulse to have sufficient energy to take most of the energy from the Ti:sapphire crystal. Otherwise, this energy will be dumped into cw lasing. In Fig.2-7 we schematically show the signal on the photodiode from the regenerative amplifier. Fig.2-7(a) shows the regenerative amplifier laser without injection. Fig.2-7(b) shows the regenerative amplifier with good injection. The pulse moves back in time, and the cw part of the wave disappears. The spike represents one pulse as it is amplified. The distance between pulses is 10ns which is determined by the cavity length. Fig.2-7(c) shows the regenerative amplifier with poor injection. In this case, the time shift is smaller, and the regenerative amplifier component is larger. Good injection will be obtained with an input power of 1W, and poor injection will occur at input energies of less than 50mW.

Besides having high enough power, it is necessary to have stable injection in order to obtain good injection. If the injection is not stable, then it will be impossible to trigger the regenerative amplifier to inject and eject the pulses at the right times.

The Pockels cell in the regenerative amplifier is switched by the electronics box PC101. This box has as its input the 76MHz signal from the Ti:sapphire laser. It divides this signal to convert it into a 1kHz signal. One signal is sent to trigger the Ti:sapphire laser. Another signal is sent to let the pulse from the stretcher in, and then eject the pulse when it has been amplified. These times are referred to as injection and ejection times. The function of the box PC101 is shown in Fig.2-8.

2.3.2 Output Beam Parameters: Spatial Chirp.

For the adiabatic rapid passage experiment that we had in mind, it was important to eliminate spatial chirp. Spatial chirp refers to the fact that different spatial elements of the beam can contain different optical frequencies. It can be observed by sending the beam into the spectrometer. There is spatial chirp if the spectrum changes as the beam input path is changed.

We found that the Mira laser had no spatial chirp associated with it. One attractive feature about the stretcher and the compressor is that they each perform their task with just one grating. In a system with two gratings, it is important to align the gratings precisely with respect to one another. Otherwise, spatial chirp may result. In the systems with one grating, since the same grating is used for input and output, the grating angle will always be correct.

The stretcher itself had a small amount of spatial chirp, which seemed to be generated by the polarizing beamsplitting cubes. This spatial chirp was removed by the regenerative amplifier, which did not show spatial chirp.

The compressor did add a spatial chirp, which we were not able to remove by adjusting the mirror system. We modified the compressor as shown in Fig.2-9, adding optics that allow us to more precisely control the input path to the compressor. On the left side of this figure, a 2m converging lens L51 has been added to the compressor. The telescope TEL29 was removed from the stretcher.

2.3.3 Output Beam Parameters: Beam Energy, Wavelength, and Temporal Length

The output of this system is a 1kHz, 200fs pulse with an energy of 200 μ J. It has a diameter of 7mm and a round shape, and is well collimated.

This pulse is intense enough to generate white light continuum in water. We temporarily digress to discuss white light continuum generation. When the high energy ultrafast pulse from the Ti:sapphire is focused into a cell containing water, then white light is generated. This white light is itself ultrafast, and can be used for spectroscopy [12, 13]. The literature does not discuss the mechanism for the production of white light. The fact that white light is generated is somewhat surprising, because water is transparent in the optical domain. One explanation for white light is that energy levels are coherently excited, and as the light propagates, there is mixing at sum and difference frequencies. If the input light is powerful and short enough, then as it propagates through the medium, the entire white light continuum is generated. It may be interesting to study the response of white light to shaped pulses [14]. In this case, the easiest thing to measure will not be the white light, but the precursor to white light [15]. We can expect to see the spectrum reshaped in different ways for different pulse shapes.

The injection is good, since there is far more than enough power in the Mira to seed the regenerative amplifier. For the same reason, aligning the system is not difficult. Because the Mira has much more power than needed for seeding, precise alignment is not necessary to obtain the initial seeding, which can then be optimized.

The wavelength of the Mira is tunable from 780nm to 830nm. The regenerative amplifier has a bandwidth of about 20nm that is centered at 805nm, and is not tunable. If the Mira pulse of 780nm is sent into the regen, the resultant pulse will be pulled

towards the red. The output amplified spectrum is slightly narrower than the Mira. The autocorrelation width of the Mira is measured with a speaker-type autocorrelator to be 250fs and the autocorrelation width of the amplified beam is measured with a single shot autocorrelator to be 240fs.

The bandwidth of the Mira pulse is 10nm, and has a Gaussian shape. The amplified Mira pulse is also Gaussian, with a width of 8nm (these widths may vary from day to day depending on the system alignment parameters). These spectra are shown in Fig.2-10.

Fig.2-11 shows the STRUT data set of an unamplified pulse from the Mira laser. The computer program to generate this figure is given in [16]. Fig.2-9(A) shows the original STRUT data set. The x-axis shows the wavelength, which is centered at 400nm because of the doubling crystal. In Fig.2-10(B), Fig.2-10(C), and Fig.2-10(D) we show the analysis of the pulse. Fig.2-10(B) shows the derivative of the phase $d\phi/d\omega$ that is recovered from the data of (A). Since this pulse is not chirped, this derivative is flat. In Fig.2-10(C) we show the intensity as a function of wavelength, which is a Gaussian. In Fig.2-10(D) we show the intensity as a function of time, which is also a Gaussian.

In Fig.2-11, we show the STRUT data set for an amplified pulse. This is somewhat distorted from the unamplified pulse of Fig.2-10. However, the fundamental shape is still the same. In the next chapter, we will show results from the STRUT for shaped pulses

2.4 Review of Pulse Shaping

Shaping ultrafast pulses is useful for experiments in communications and quantum control. Shaping ultrafast pulses is not trivial, because there are no electronic devices that can work on this time scale. Therefore, the technique of indirect pulse shaping, which includes LCM pulse shaping [17-20], AOM pulse shaping [9, 21, 22], and time-stretched pulse shaping [23], is used. The choice of which pulse shaping apparatus to use may depend on the particular application; each technique has different advantages to it. We will show data from previous pulse shaping experiments, which can be compared to the data that we will present later in this thesis.

Pulse shaping in the RF domain has been used extensively by NMR scientists. In this case, the pulse lengths are on the order of μs . Such pulse shaping has enabled NMR scientists to demonstrate effects such as adiabatic rapid passage, and to study molecular structure and dynamics.

It was then desired to extend this technique into the optical domain. Optical pulse shaping has many intriguing applications, as described in [9], such as breaking strong bonds [24], selectively populating highly excited vibrational states of anharmonic ladders [25], manipulating curve crossings between states [26], and suppressing intramolecular vibrational relaxation [27]. It should be noted that there are will also arise difficulties in exciting atoms with optical pulses that do not arise in the rf domain. An example of this is pulse reshaping. As an optical pulse propagates through an optically dense medium, it will become reshaped [28]. This is a phenomena that would not be observed in the rf domain, because of the long rf wavelength. However, such phenomena are themselves interesting.

Shaping fs pulses in the optical domain is more technically challenging than shaping μs pulses in the rf domain. If the optical pulse that we wish to shape has a temporal duration of fs or ps, then we will need a modulator that works on this time scale. The idea of shaping a pulse by sending it through a modulator, such as a Mach-Zehnder, is referred to as direct pulse shaping. Current modulators [29] can operate at 60GHz, which is much slower than necessary to shape a femtosecond pulse.

A creative solution to the problem of slow modulators is the technique of indirect pulse shaping. This concept can be seen in Fig.2-13. The pulse is spread by a grating, so that each different spectral component maps onto a different spatial position. By using the 4-F configuration, the beam is collimated, and in the center of the 4-F system, an element is placed that will modulate the spectrum. With this approach, it is not necessary to even have modulators in the system to shape the ultrafast pulse.

The first demonstration of indirect pulse shaping used a fixed spatial mask, a technique that does not have programmability [30]. The spatial mask can be created using lithographic techniques as in semiconductor processing. The fact that the spatial mask cannot be changed in real time limits the utility of this technique. This approach does have the advantage that it is simple, and requires no pulse picker. However, as we will discuss later, fixed mask pulse shaping proved to be a useful diagnostic tool.

Another approach uses an LCM (liquid crystal modulator) [17-20]. The LCM does not diffract the light, but just lets it pass through, as in a spatial mask. The LCM consists of discrete pixels, and the index of refraction can be changed for each pixel. The typical number of pixels is 128. One ramification of the discrete pixels is that there may be interpixel gaps that cause undesirable distortions. However, this problem has been

greatly reduced in recent work, through the use of microlens arrays and advances in LCM technology [18]. Another point is that with a single LCM, only the phase of the signal (in the spectral domain) can be modulated. To modulate both phase and amplitude, two LCM's will be required. The LCM has a refresh rate of several ms. One useful feature of the LCM is that the modulation pattern is static, and does not propagate as in the AOM, which is discussed below. The LCM and AOM technologies each have different features, and the decision on which one to use will depend on the particular application. An experimental result for the LCM work is shown in Fig.2-14 [19]. This data was taken using temporal cross-correlation. It can be seen that this data has shows excellent resolution and a high contrast ratio. However, as mentioned earlier, the contrast ratio may be somewhat misleading, since a 2nd harmonic crystal was used to make this measurement. This data was taken for the case of the unamplified pulse; the work presented in this thesis is for the amplified pulses. We also note that work has been done with an amplified pulse system followed by a LCM pulse shaper [20]. This work has been applied to excitation of a molecule, and is quite relevant to the work that we will present in this thesis. It will be discussed in more detail in the next chapter.

The AOM pulse shaping technology [9, 21, 22] uses an AOM placed at the center of the 4-F system. A tellurium-dioxide AOM is used to generate spatial modulation on the spectrum image, thus the spectral modulation. A RF (radio frequency) wave generated by a arbitrary function generator is mixed with a carrier, as described below, to produce the desired RF pulse shape. The AOM has 50x2.3mm² clear aperture size. The full width at half maximum on the spectrum is approximately 30mm on the AOM, with the

exact number depending on the focal length of the lens in the 4-F geometry, and the spectral width of the Ti:sapphire laser.

A fundamental difference between AOM and LCM pulse shaping is that the AOM will diffract the input light, with the diffraction determined by the input RF wave to the crystal. In contrast, the LCM will transmit the light, not diffract it. The fact that the AOM diffracts the light will mean that very high contrast ratios can be obtained in AOM pulse shaping. The contrast ratio will be determined by the contrast ratio of the RF wave. The RF electronics that we use are specified to have a contrast ratio of 40dB. The RF wave propagates across the crystal, so that the temporal RF wave is mapped onto the spatial dimension of the crystal. The mathematics of this will be discussed in later chapters. The diffraction angle is determined by the sum of the optical wave vector and the acoustic phonon vector. The output wave will be the product of the acoustic wave (in the spatial domain) and the optical wave.

The RF wave propagates at the speed of sound in the crystal, which is approximately $v=4\text{mm}/\mu\text{s}$. Light travels at the much faster speed of $2\times 10^5\text{ mm}/\mu\text{s}$ (in the crystal). This difference in speed means that the acoustic wave is stationary with respect to the optical wave. Thus, at the time in which the pulse passes through the AOM, the AOM acts as a stationary mask. It should be noted that the AOM is a continuous medium, unlike the LCM, which consists of discrete pixels. The number of possible features in the AOM is given by: $N=L\times(A/v)$. In this equation, L is the crystal length, which is 4cm, v is the velocity of sound in the crystal, and A is the center modulator frequency, which in this case is 200MHz. The term v/A gives the minimum feature size to be approximately $21\mu\text{m}$, and so $N=1900$.

To achieve a spatial resolution of 21 μ m, the input beam must be expanded. The Ti:sapphire laser has a spot size of 3mm, and is expanded by a telescope to a size D . To focus it into a spot of size $d=21\mu\text{m}$, with a lens of focal length $F=30\text{cm}$, then $D=\lambda F/d=3\text{cm}$. This determines the telescope that must be used before the pulse shaper.

The RF wave consists of a carrier wave, which will diffract the light, modulated by a lower frequency signal wave. The setup for the RF electronics is shown in Fig.2-15. The function generator produces the 200MHz carrier wave. This carrier wave is sent into a 90° splitter, which splits it into real and imaginary components. The arbitrary function generator will produce two RF waves, with a modulation of approximately 30MHz. One wave generated by the arbitrary function generator will correspond to the real part of the RF signal, while the other wave will correspond to the imaginary part. The arbitrary function generator is then mixed with the 200MHz carrier, and recombined with a 0° combiner. With this RF setup, the real and imaginary parts, or equivalently, the amplitude and phase, of the RF pulse can be arbitrarily chosen. Since the output optical pulse will have its phase and amplitude determined by the RF pulse, this means that the AOM is capable of shaping the optical pulse with arbitrary amplitude and phase.

In Fig.2-16, we show the RF wave that is sent into the AOM. In this case, the RF wave was chosen as a series of on-off pulses. The resultant optical pulse (in the temporal domain) is shown in Fig.2-17 (the data in Fig.2-16 and Fig.2-17 is from [9]). The dotted line in this figure is the theoretically predicted result and it can be seen that it agrees well with the experiment. It shows a complex waveform with high resolution and high contrast ratio.

Pulse picking is necessary in AOM pulse shaping, and is described in Fig.2-18. Fig.2-18a shows the RF wave with two features imposed upon it. Figure 2-18b shows the unmodulated spectrum of the signal. Fig.2-18c shows the result of putting the RF signal onto the pulse at a time T_1 . At a later time T_2 , the RF signal will have propagated in the AOM, and the features A and B will appear at different wavelengths. Thus, if we want to be able to create an AOM signal that can appear at a desired wavelength, it will be necessary to have a pulse picker in the system. In the system that we will describe in later chapters, the pulse picker is the Pockels cell inside the regenerative amplifier.

The Ti:sapphire operates at 76MHz, and if we use an AOM, then because of the pulse picker arrangement, we will only get pulses at a rate of 1MHz. If an LCM is used, then it will be possible to get pulses at 76MHz. However, in the amplified pulse shaper, the limiting speed is the 1kHz repetition rate of the Nd:YAG laser. Thus, in the case of amplified pulse shaping, the AOM modulator and the LCM modulator perform equivalently.

The AOM has an updating time given by $t=L/v$, or $t=10\mu\text{s}=0.01\text{ms}$. The LCM has a slower refresh rate than the AOM, which may make the AOM more useful for certain communications applications. The LCM has an update rate of about 10ms, which is much slower than the AOM, which has an update rate of 0.01ms. The slow refresh rate does not mean that the LCM array has no communications applications. The LCM has the advantage that no pulse picker is required, because there is no propagating wave. It may be useful for the case where a user wants to put the same code onto each pulse, as a form of identification.

To summarize the comparison between LCM and AOM technologies, we include the following table:

	AOM	LCM
Method of shaping	Diffraction	Transmission
Update rate	100kHz	100Hz
Phase and Amplitude?	1 AOM can modulate both phase and amplitude	To modulate both phase and amplitude, 2 modulators are required.
Number of features	>1000	128
Cost	\$3,000	\$10,000
Discrete pixels?	No	Yes
Needs pulse picker?	Yes	No

Pulse shaping has also been accomplished by using stretcher technology to stretch the pulse in time [23]. Then, an electro-optic modulator (with GHz speed) can be used to modulate the pulse, and the pulse is then recompressed. The work of [23] was done by modulating only the pulse amplitude; however, it could be extended to both the amplitude and phase domains. This pulse shaping technique is more difficult to achieve experimentally than the LCM and the AOM techniques. It requires modulators that work at speeds of 20GHz, and arbitrary function generators that can also achieve this speed. In contrast, the arbitrary function generators that we use for the AOM pulse shaping work at 200MHz.

Finally, we note that workers in this lab have accomplished pulse shaping at a wavelength of $1.55\mu\text{m}$, using a mode-locked fiber laser and AOM technology. This work has demonstrated pulse shaping in time as well as wavelength [32, 33].

2.5 References

1. Bern Kohler, V. V. Yakovlev, Kent R. Wilson, Jeff Squier, Kenneth W. DeLong, and Rick Trebino, "Phase and Intensity Characterization of Femtosecond Pulses from a Chirped-Pulse Amplifier by Frequency-Resolved Optical Gating," *Opt. Lett.*, **20**, 483-485 (1995).
2. J-K. Rhee et al, "Real-time Dispersion Analyzer of Femtosecond Laser Pulses with use of a spectrally and temporally resolved upconversion technique", *J. Opt. Soc. Am. B*, **13** : 8 (1996).
3. J-K. Rhee, T.S. Sosnowski, T.B. Norris, J.A. Arns, W.S. Colburn, "Chirped-Pulse Amplification of 85-fs Pulses at 250 KHz with 3rd-Order Dispersion Compensation by use of Holographic Transmission Gratings," *Optics Letters*, **19**, 1550-1552 (1994).
4. D.N. Fittinghoff, J.L. Bowie, J.N. Sweetser, R.T Jennings, M.A. Krumbugel, K.W. DeLong, R. Trebino, "Measurement of the intensity and phase of ultraweak, ultrashort laser pulses," *Optics Letters*, **21** (12) (1996).
5. C. Iaconis, I.A. Walmsley, "Self-Referencing Spectral Interferometry for Measuring Ultrashort Optical Pulses," *IEEE Journal of Quantum Electronics*. (to be published, 1999).
6. L. Jusinski, <http://www.ca.sandia.gov/ultrafrog/>
7. A. Siegman. *Lasers*. University Science Books, 1986.
8. R. Danielius, et al. "Characterization of phase modulated ultrashort pulses using single-shot autocorrelator", *Optics Communications*, **105** :2 p.167 (1994).

9. J.X. Tull, M.A. Dugan, W.S. Warren, "High-Resolution Ultrafast Laser Pulse Shaping and Its Applications," *Advances in Magnetic and Optical Resonance*, **20** (1997).
10. XJ-400 Laser Manuals. (unpublished). CLARK-MXR Inc. 7300 West Huron River Drive, Dexter, MI 48130.
11. S. Kane, "High-Order Dispersion Control for the Amplification and Compression of Femtosecond Laser Pulses". PhD Thesis, University of Michigan (1996).
12. T. Asahi, A. Furube, H. Fukumura, M. Ichikawa, H. Masuhara, "Development of a femtosecond diffuse reflectance spectroscopic system, evaluation of its temporal resolution, and applications to organic powder systems," *Review of Scientific Instruments*, **69**: 361-371 (1998).
13. A. Hertwig, H. Hippler, A.N. Unterreiner, P. Vohringer, "Ultrafast relaxation dynamics of solvated electronics in water," *Berichte der Bunsen-Gesellschaft-Physical Chemistry Chemical Physics*," **102**: (6) 805-810 (1998).
14. W.S. Warren, conversation (1998).
15. I.A. Walmsley, conversation (1998).
16. D. Keusters, "Towards Quantum Control: Generation, Amplification, and Characterization of Shaped Ultrafast Laserpulses". (1998, unpublished).
17. K.M. Mahoney, A.M. Weiner, "A femtosecond pulse-shaping apparatus containing microlens arrays for use with pixellated spatial light modulators", *IEEE J Quantum Elect* **32**: (12) 2071-2077 (1996).
18. Wefers MM, Nelson KA, Weiner AM, "Multidimensional shaping of ultrafast optical waveforms", *Optics Letters* **21**: (10) 746-748 (1996).

19. A.M. Weiner, <http://dynamo.ecn.purdue.edu/~amw/>
20. A. Assion, T. Baumert, M. Bergt, T. Brixner, B. Kiefer, V. Seyfried, M. Strehle, G. Gerber, "Control of Chemical Reactions by Feedback-Optimized Phase-Shaped Femtosecond Laser Pulses," *Science* **282** 919 (1998).
21. Dugan MA, Tull JX, Warren WS, "High-resolution acousto-optic shaping of unamplified and amplified femtosecond laser pulses," *J Opt Soc Am B* **14**: (9) 2348-2358 SEP 1997.
22. J.X. Tull, The Development of High Resolution Ultrafast Laser Pulse Shaping Techniques, PhD Thesis (Princeton University, 1996).
23. M. Haner, W.S. Warren, "Synthesis of crafted optical pulses by time domain modulation in a fiber-grating compressor," *Appl. Phys. Lett.* **52** , 1458 (1988).
24. S. Shi, H. Rabitz, *Journal of Chemical Physics*, **92**, 2927 (1990).
25. J.S. Melinger, D. McMorro, C. Hillegas, W.S. Warren, *Phys. Rev.A*, **51**, 3366.
26. P. Gross, D. Neuhauser, H. Rabitz, *Journal of Chemical Physics*, **96**, 2834 (1992).
27. D. Goswami, W.S. Warren, *Journal of Chemical Physics*, **99**, 4509 (1993).
28. L. Allen, J. H. Eberly, *Optical Resonance and Two-Level Atoms* (Dover Publications, 1987).
29. W.S. Wang, D.T. Chen, H.R. Fetterman, Y.Q. Shi, W.H. Steier, L.R. Dalton, P.M. Chow, "Optical Heterodyne-Detection of 60 GHz electrooptic modulation from polymer wave-guide modulators", *Applied Physics Letters*, **67**: (13) 1806-1808 p.25 (1995).
30. A.M. Weiner, J.P. Heritage, R.N. Thurston, *Optics Letters*, **11**, 153.

31. W. Yang, F. Huang, M. R. Fetterman, D. Goswami, W. S. Warren, "Demonstration of Amplitude Feedback in an Ultrafast Pulse Shaping System at 1.55 μ m," *Opt. Lett.* (1999) (to be published).
32. W. Yang, J. Davis, D. Goswami, M. R. Fetterman, W. S. Warren, "Optical wavelength domain code-division multiplexing using AOM-base ultrafast optical pulse shaping," *All-Optical Networking: Architecture, Control, and Management Issues*, SPIE Vol. 353 (1998).

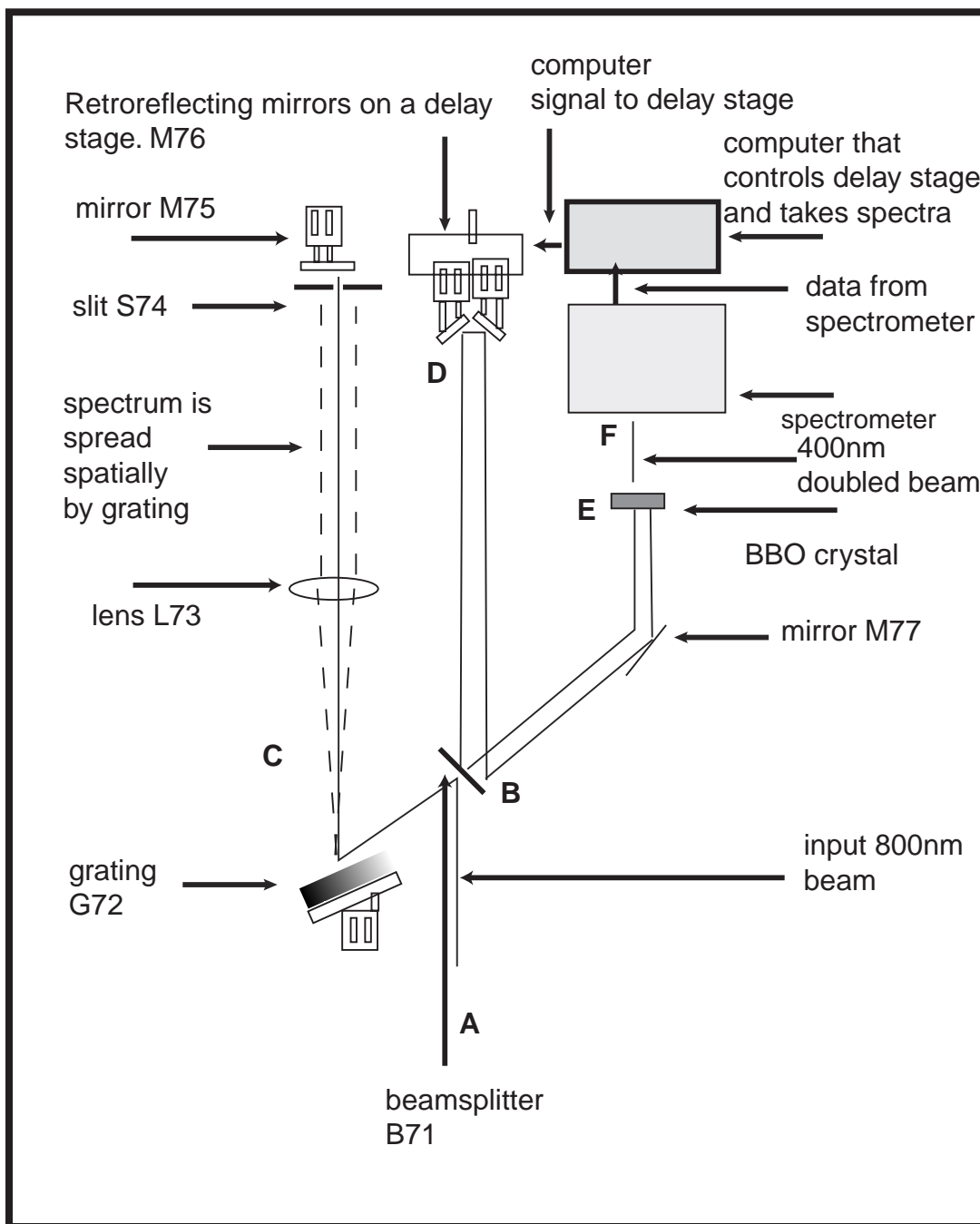


Figure 2-2.

STRUT Schematic. (A) The input 800nm pulse enters the system. (B) It is split into two beams, probe and reference. (C) The reference is spectrally filtered. (D) The probe travels to a delay stage. (E) the beams combine in a nonlinear crystal. (F) a spectrometer detects the signal

[m65]

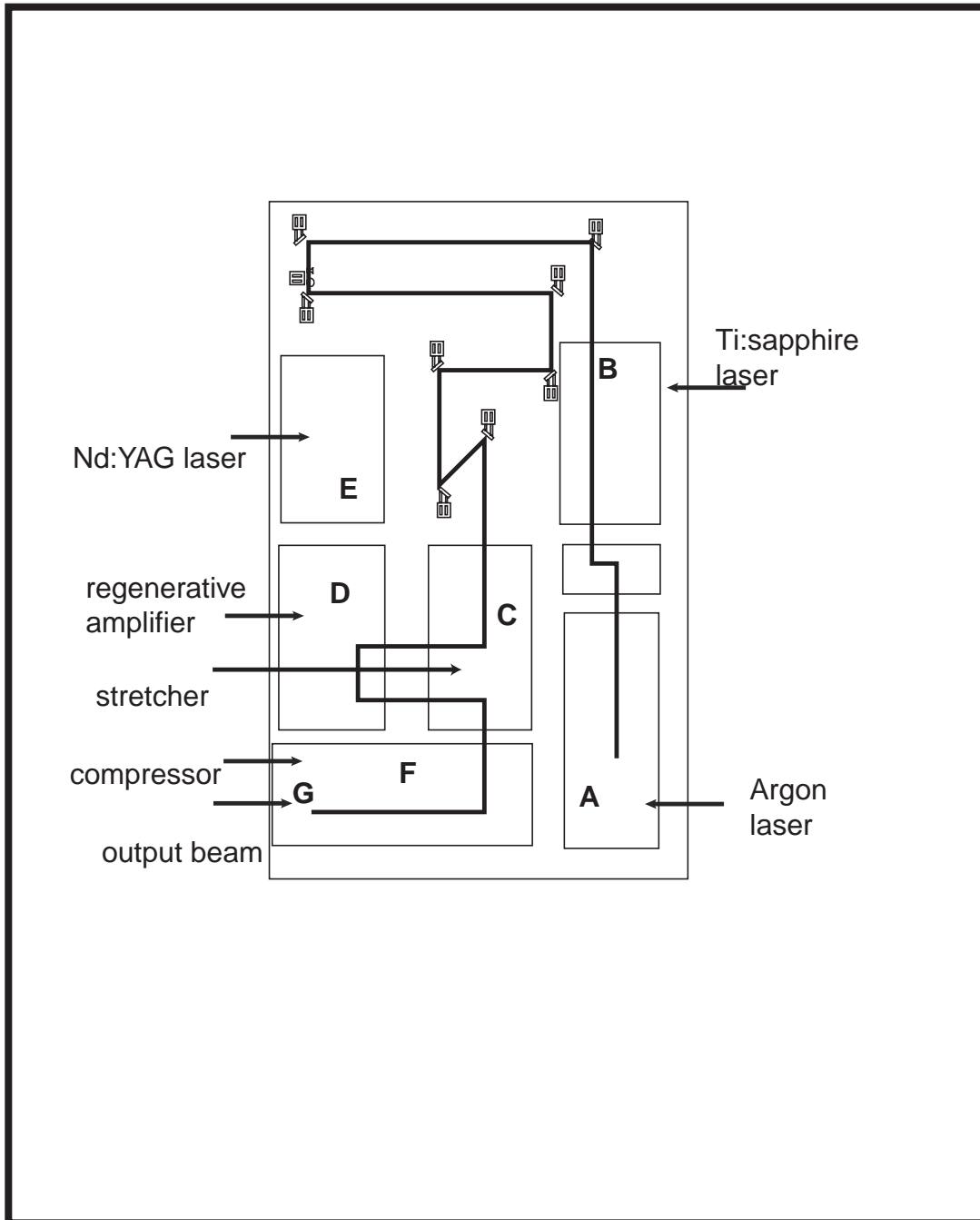


Figure 2-4

the amplified pulse shaping system. argon laser pumps ti:sapphire laser. then the beam goes into stretcher, regenerative amplifier, compressor.

[opo12]

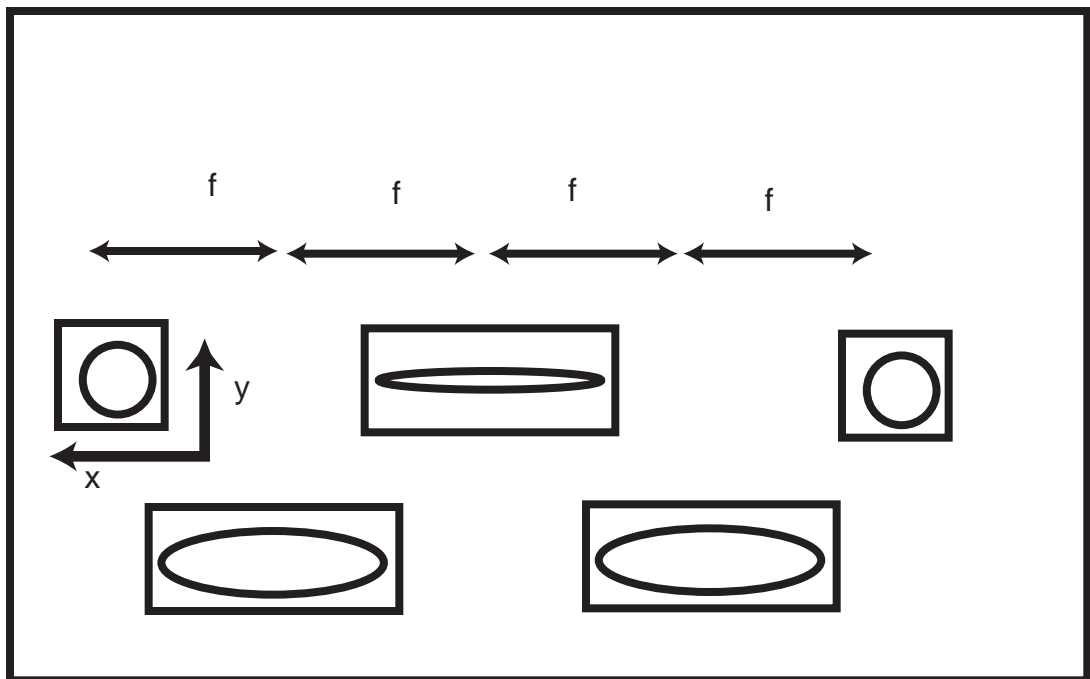
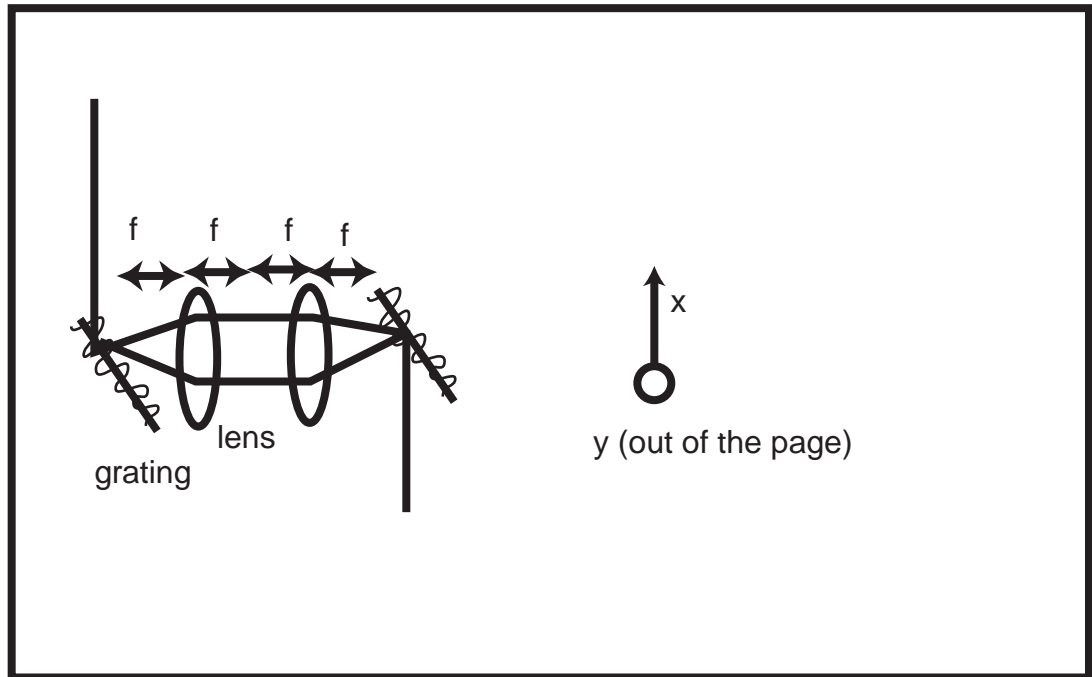


Figure 2-5.
 a) top, the schematic of the 4-F system. Input grating, two lenses, and another grating to recombine the beam spatially.
 b) the transverse beam as it propagates [a601]

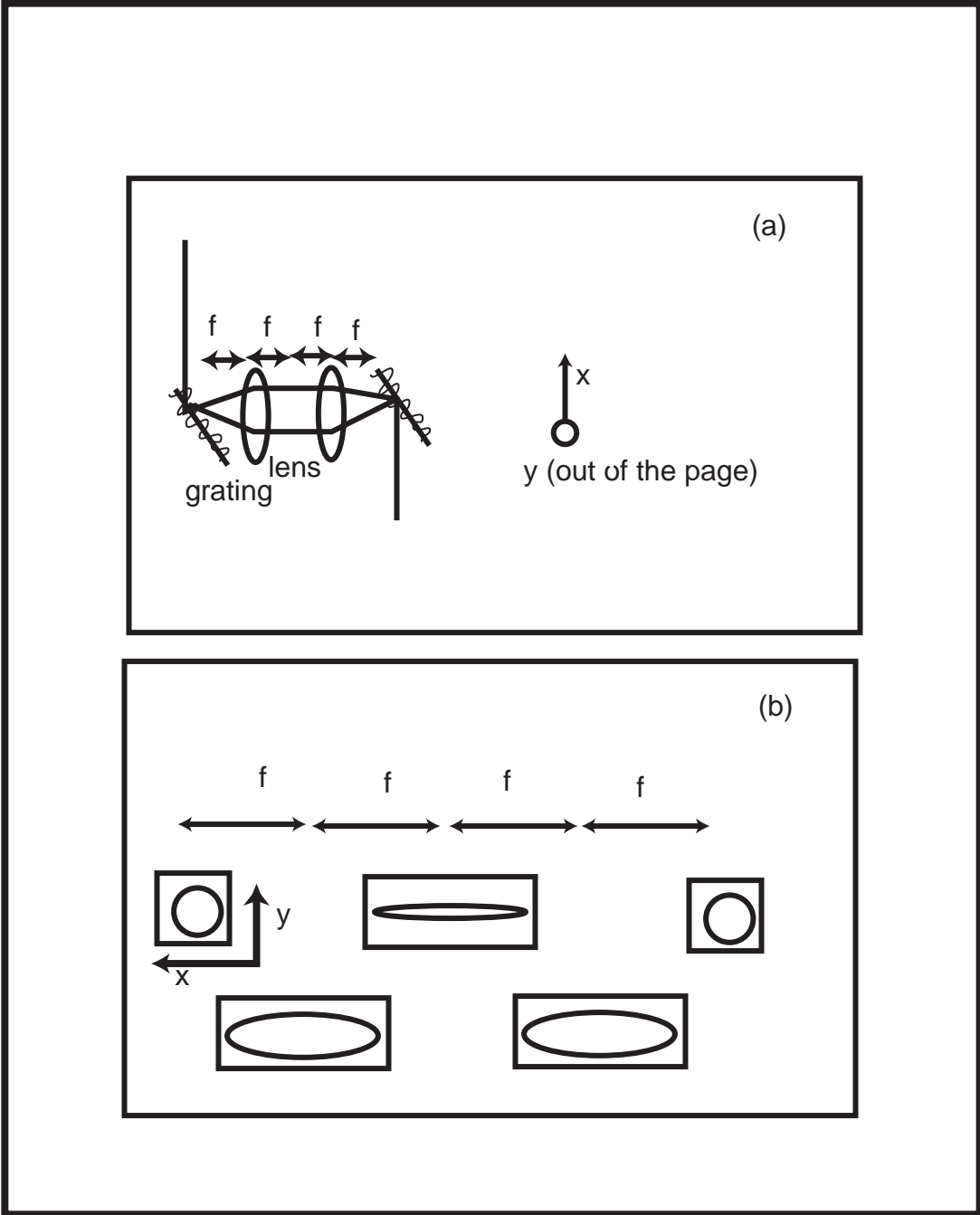


Figure 2-6.

a) the schematic of the 4-F system. Input grating, two lenses, and another grating to recombine the beam spatially.

b) the transverse beam as it propagates [op15]

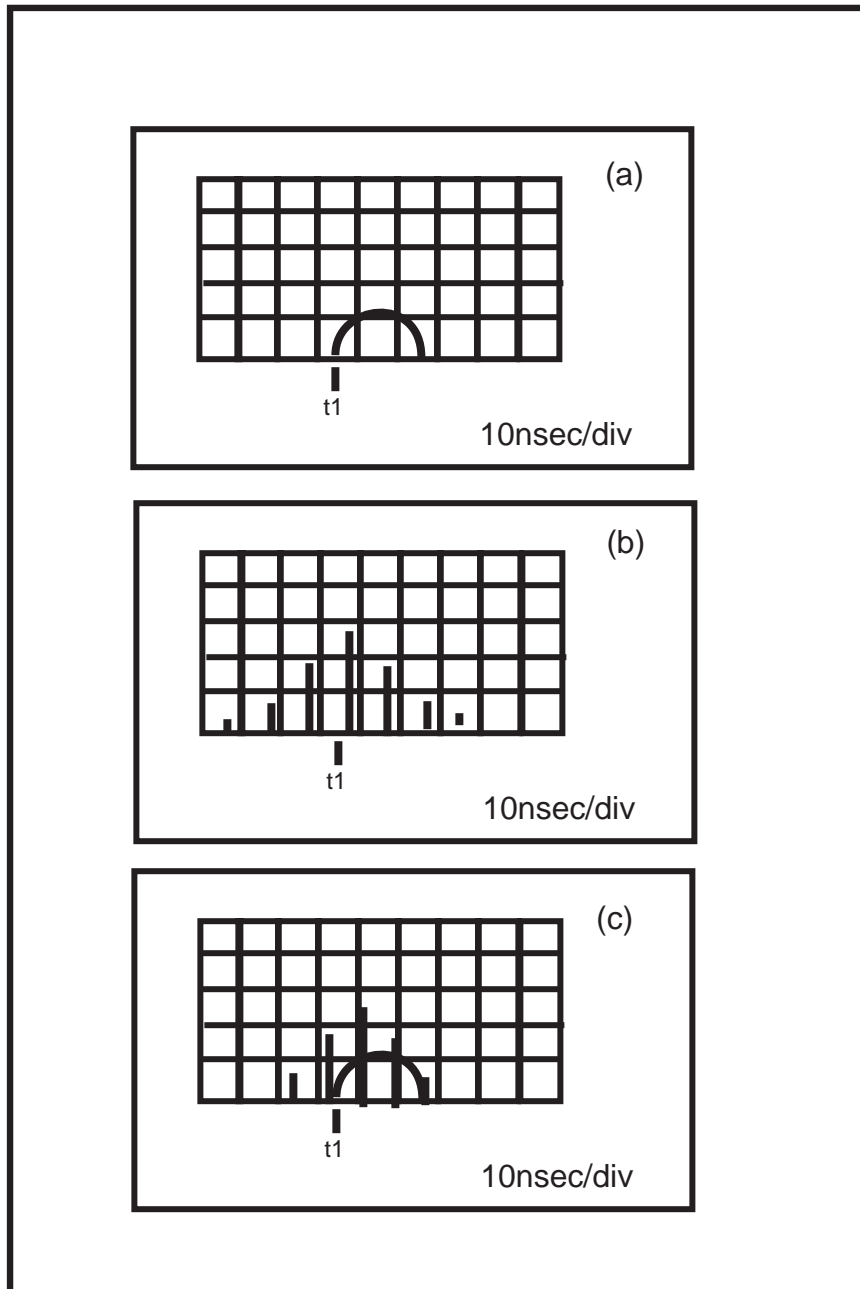


Figure 2-7.

These figures show the oscilloscope display from a photodiode studying the regenerative amplifier.

(a) no injection, just the cw signal. **(b)** good injection. the cw signal disappears. the peaks are from the injected pulse. the peaks are separated by 10ns. they rise and fall. Under real conditions the pulse would be ejected from the regen at its peak. **(c)** poor injection. if the seed pulse does not have enough energy then injection is poor. We will see the cw signal and the seed pulse injection.

[ar123]

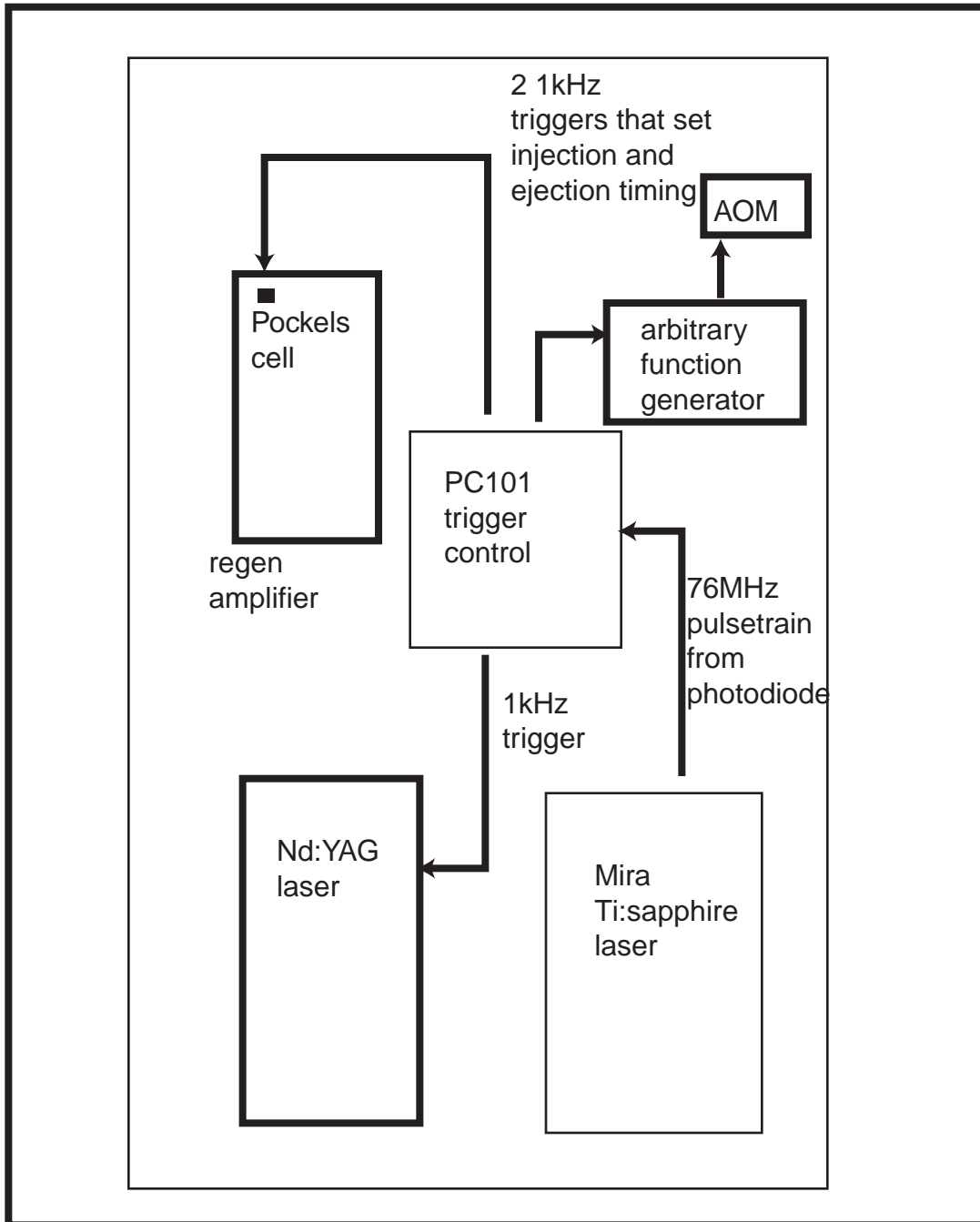


Figure 2-8.

trigger setup. The control box PC101 received the signal of the Ti:sapphire modelocked pulse train. It then divides this signal into a 1kHz pulsetrain to trigger the Nd:YAG laser and the Pockels cell. It also triggers the arbitrary function generator, which is discussed in Chapter 3.

[u533]

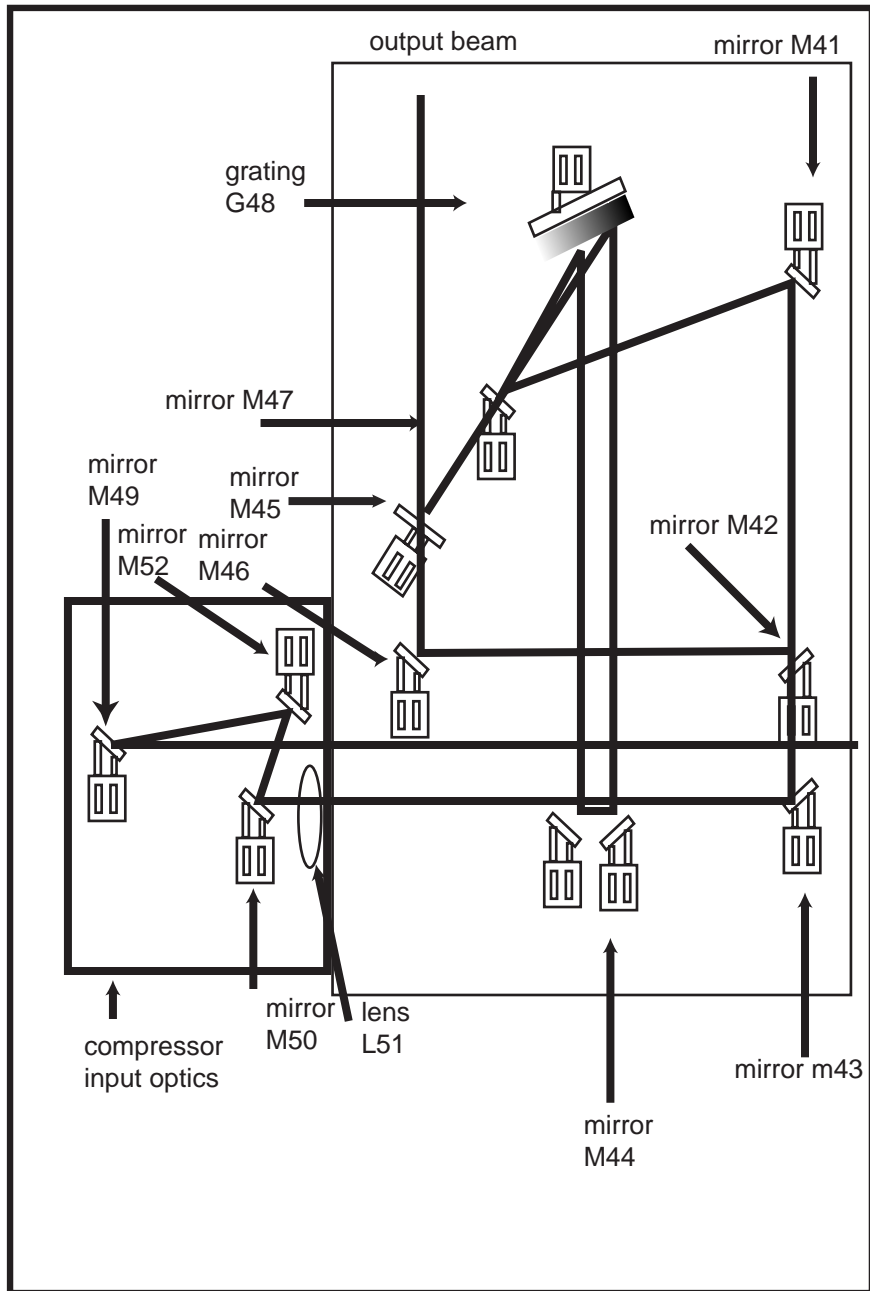


Figure 2-9.
 the modified compressor layout. The compressor input optics on the left
 reduce spatial chirp.

[xx3]

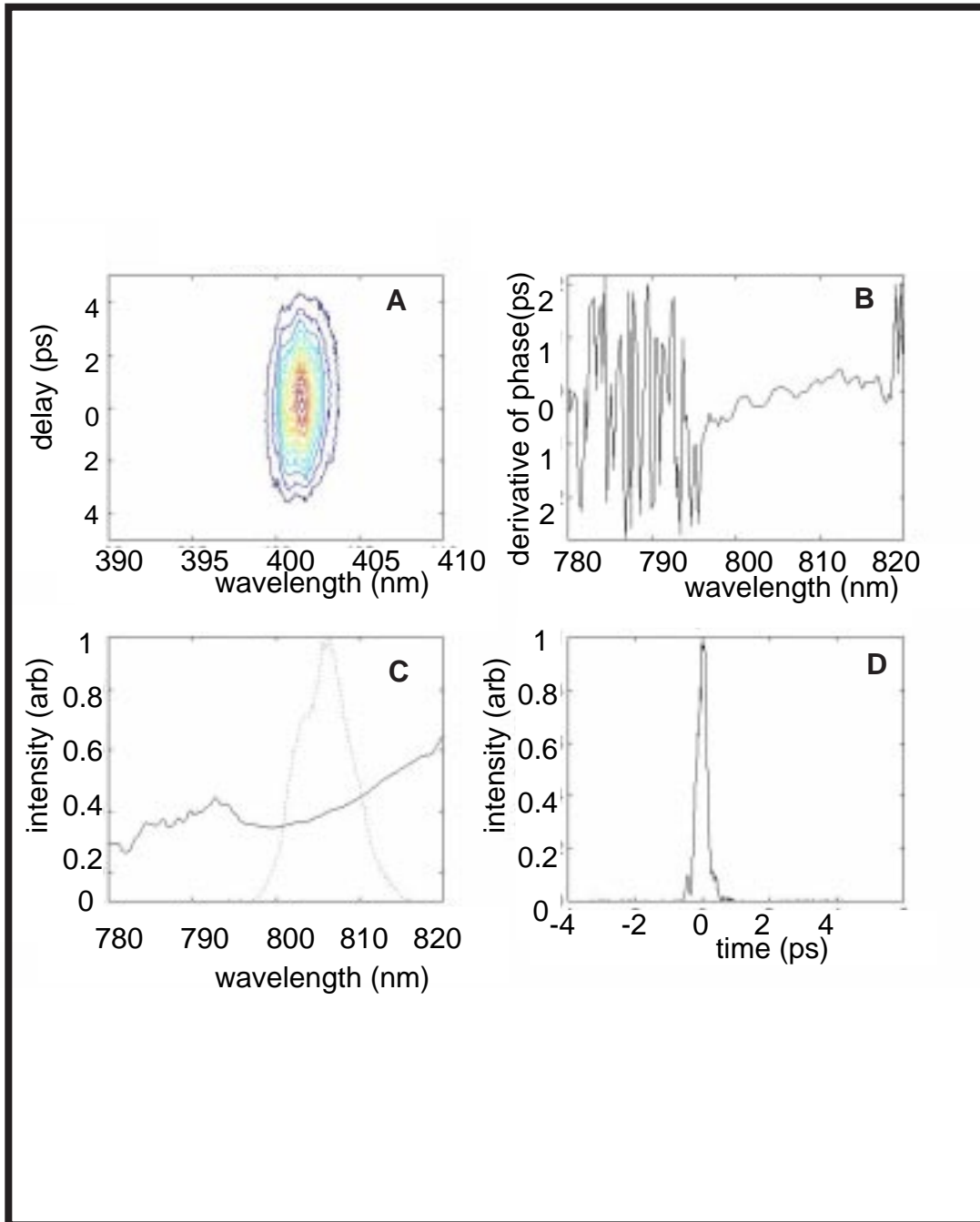
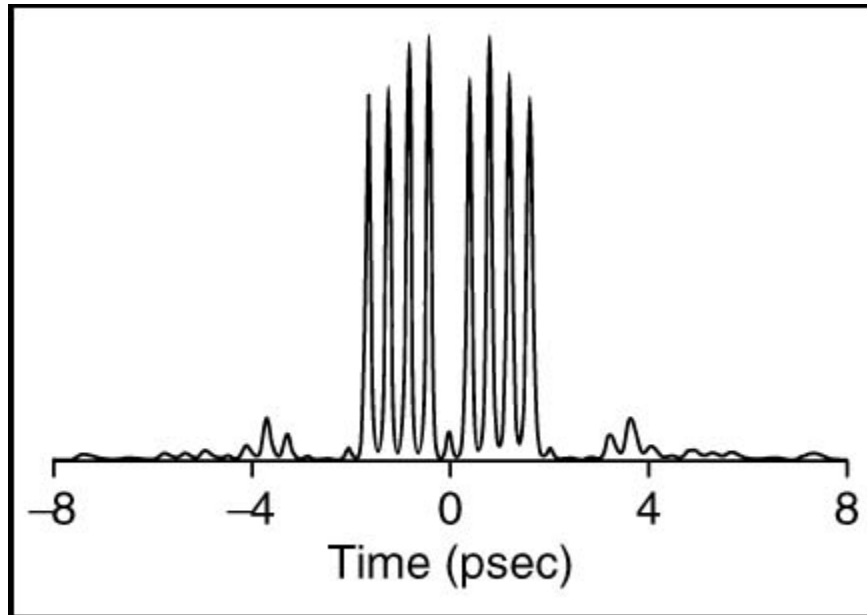


Figure 2-11.

STRUT data. **(A)**STRUT of the Ti:sapphire pulse from the Mira laser. **(B)** derivative of the phase recovered from **A**. **(C)** intensity of the pulse as a function of wavelength. **(D)** intensity of the pulse as a function of time.

[qy11]



Purdue University Ultrafast Optics Group

Figure 2-14.

Pulse shaping demonstration with an LCM modulator. [A. Weiner, see text for reference]. [loki13]

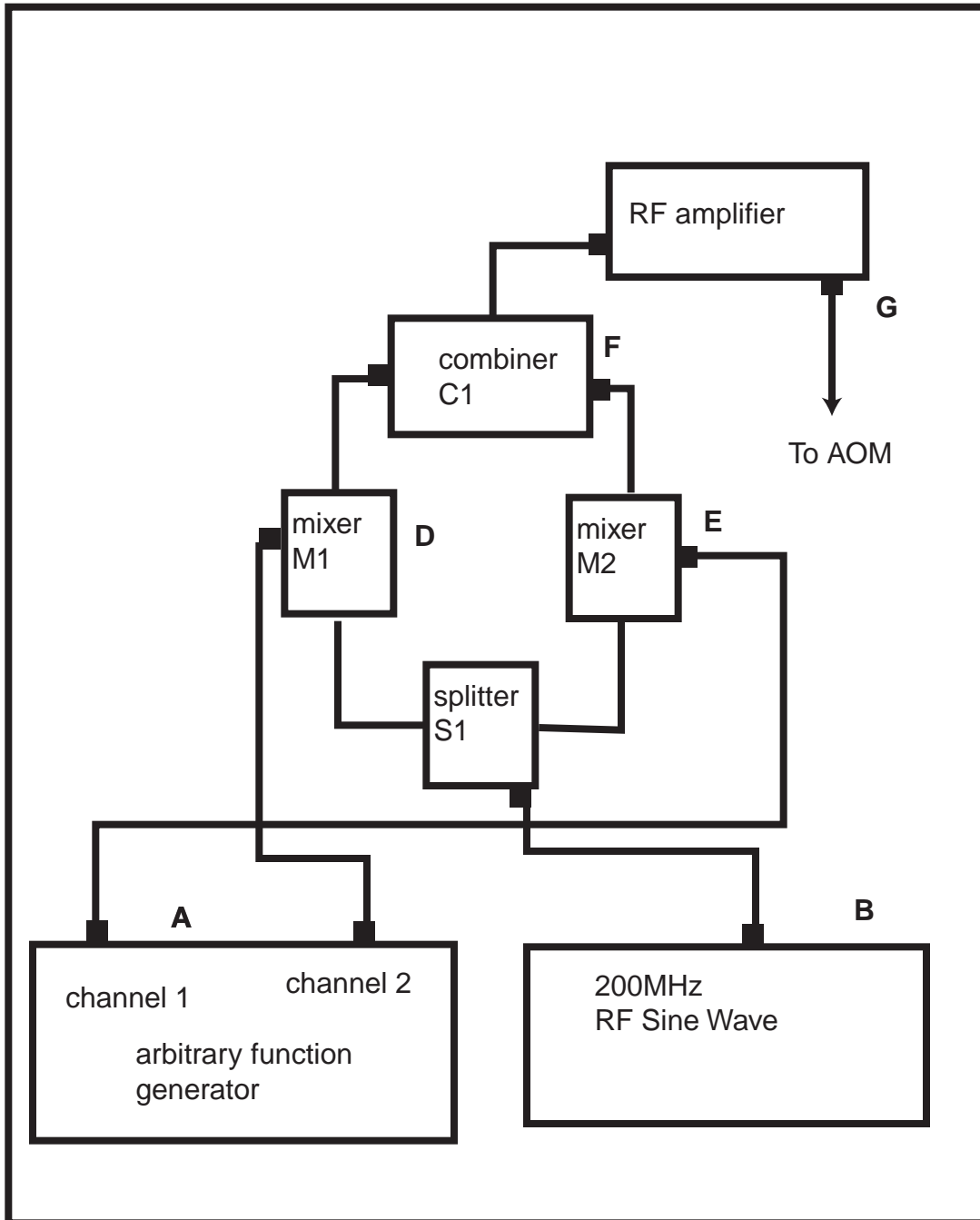


Figure 2-15.

RF Circuitry for the AOM. The arbitrary function generator produces a shaped pulse in two channels, real and imaginary (A). The 200MHz sin wave (B) is split into real and imaginary components (C). This is then mixed with the arbitrary function (D,E). The RF wave is then sent into the combiner (F), amplified, and then goes to the AOM (G).

[po56]

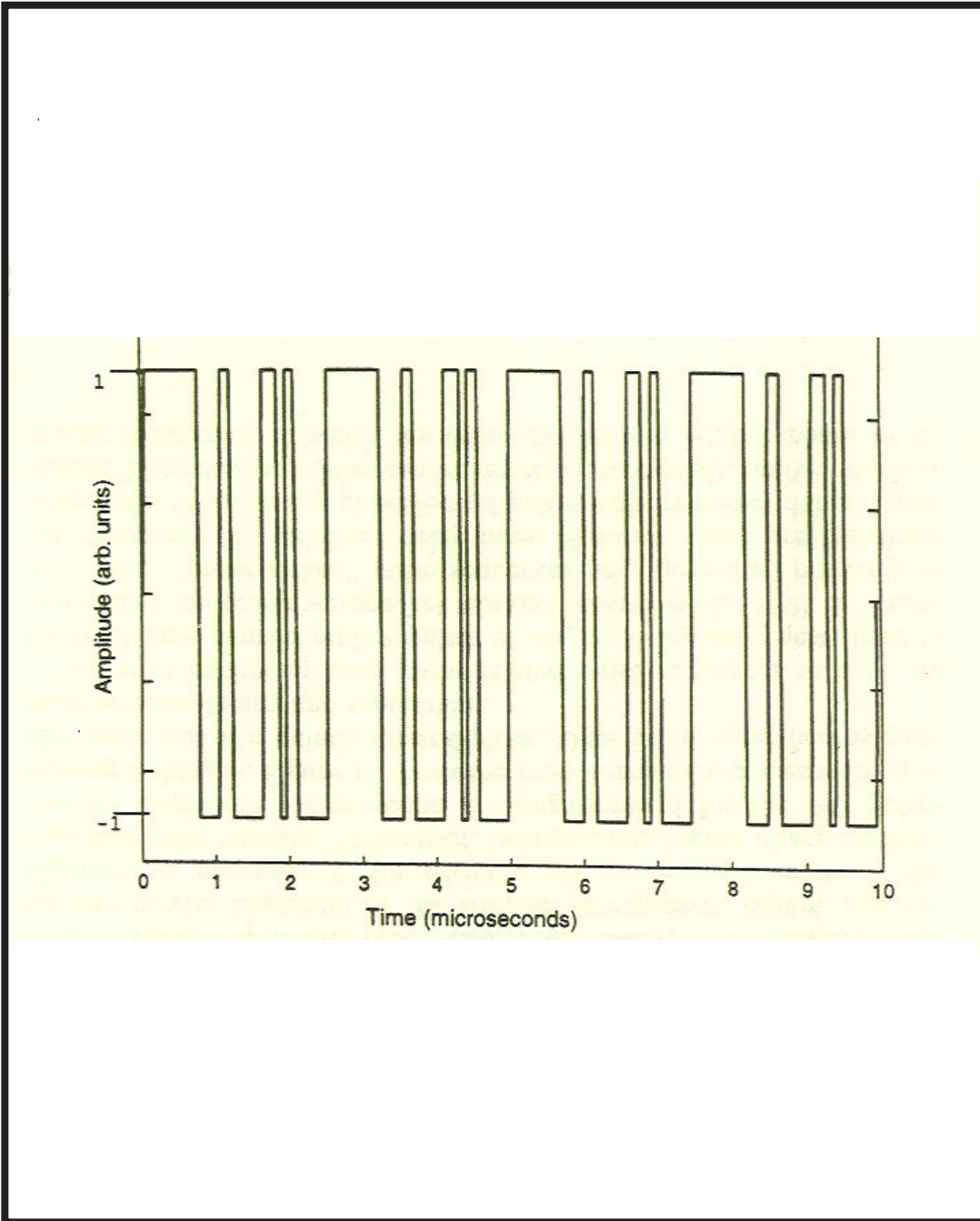


Figure 2-16.

Previous demonstration of AOM pulse shaping. The applied RF signal used to create the optical waveform of Fig.2-17. [J.X. Tull et al, see text for reference].

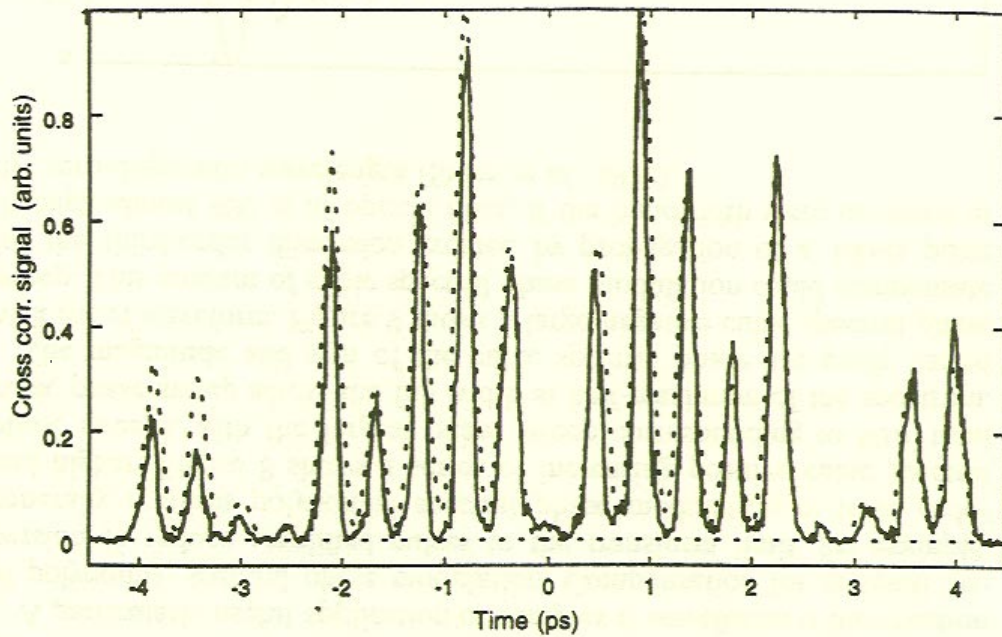


FIG. 6. Experimental (solid) and theoretical (dashed) cross-correlations resulting from a sequenced pattern of binary π spectral phase shifts.

Figure 2-17.

Previous demonstration of AOM pulse shaping. The measured cross-correlation signal. [J.X. Tull et al, see text for reference].

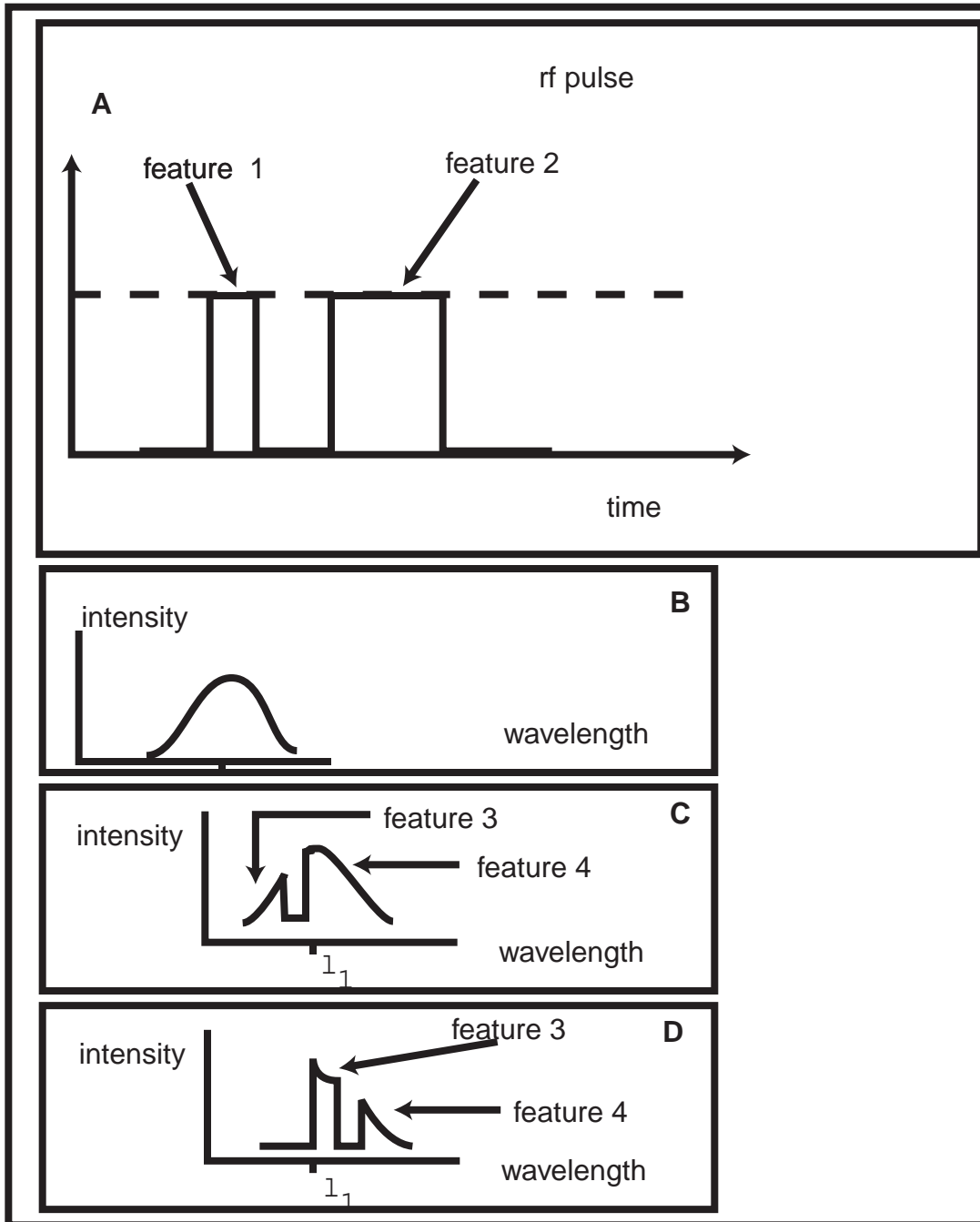


Figure 2-18.

The AOM pulse shaper requires a pulse picker and synchronization. (A) this shows the RF pulse with two features imposed upon it. (B) This shows the unmodulated optical pulse. (C) This shows the modulated pulse at time T_1 . Feature 3 and feature 4 come from feature 1 and feature 2 in the RF pulse. (D) At a later time T_2

[nd48]